

ORIGINAL ARTICLE

Fabrication of large-area and high-crystallinity photoreduced graphene oxide films via reconstructed two-dimensional multilayer structures

Yuanlong Shao¹, Hongzhi Wang¹, Qinghong Zhang¹ and Yaogang Li²

Graphene, the last representative sp^2 carbon material to be isolated, acts as an ideal material platform for constructing flexible electronic devices. Exploring a new method to fabricate high-quality graphene films with high throughput is essential for achieving greater performance with flexible electronic devices. Here, we report a facile coating and subsequent illumination method for mass-fabricating highly crystalline photoreduced graphene oxide (PRGO) films directly onto conductive substrates. The direct fabrication of PRGO films onto Cu foils with partial oxygenated groups, an intensive stacked highly crystalline structure, and reduced graphene oxide regions enable significant performance enhancements when used as supercapacitor electrodes compared with other graphene-only devices, exhibiting high specific capacitances of 275 F g^{-1} at a scan rate of 10 mV s^{-1} and 167 F g^{-1} at 1 V g^{-1} with excellent rate capability. The as-established all-solid-state flexible supercapacitors exhibit superior flexibility and robust mechanical stability, resulting in a capacitance delay of only 2% after performing 100 bending cycles. The demonstrated PRGO films provide a promising material platform to realize a broad range of applications related to flexible electronics devices.

NPG Asia Materials (2014) 6, e119; doi:10.1038/am.2014.59; published online 15 August 2014

INTRODUCTION

Flexible electronic devices have garnered considerable attention because of the benefits enabled by large-area, lightweight, flexible electrode films, which have the potential to enable unique advances in future mobile applications, such as wearable displays, roll-up solar cells, electronic skin and flexible energy storage.^{1,2} Graphene films containing a few layers or multiple layers of two-dimensional graphene sheets are prominent contenders as attractive components for use in flexible electronic devices due to their high conductivity, chemical stability and mechanical flexibility.^{3,4} For the practical applications of graphene in these fields, scalable production of macroscopic-scale graphene films is required rather than the current micrometer-sized graphene sheets. To date, the synthesis of large-scale flexible graphene films has mainly been demonstrated by two approaches. One approach is the 'bottom-up' synthesis strategy, by which high-quality graphene can be prepared using chemical vapor deposition to grow graphene at high temperature, followed by a transfer procedure to place graphene films onto flexible substrates;⁵ however, this method is not sufficiently cost- and time-effective to be commercially viable for mass production and requires a difficult post-functionalization step to produce the appropriate graphene films. Another approach is the 'top-down' method, that is, solution

processing of chemically exfoliated graphite, which offer advantages for continuous large-scale production and effective functionalization for particular applications. Recently, many effective solution-processing methods have been presented, such as spray-coating,⁶ rod-coating,⁷ spin-coating,⁸ the layer-by-layer technique,⁹ the Langmuir-Blodgett technique,¹⁰ interfacial self-assembly¹¹ and vacuum filtration,¹² all of which indicate the feasibility of wet-chemical methods to prepare large-area graphene films, thereby allowing graphene-based devices to be fabricated on virtually any surface. However, the application of these methods is usually limited by the difficulties in preparing large-area, high-quality graphene films, which is specifically due to the inefficiency of the homogeneous arrangement of graphene sheets and the appropriate chemical reduction of graphene oxide (GO) films. These defects hamper the orderly arrangement and effective interlinking of the individual graphene sheets, which results in uncontrollable deep wrinkles and pores in these graphene films. Therefore, the development of a rapid and low-cost method for preparing flexible, large-scale and high-quality graphene films under mild conditions remains a challenge.

Herein, we report a scalable and solution-processable strategy for assembling GO sheets directly onto conductive substrates (for example, Cu foil) and subsequently reduce the GO sheets into highly

¹State Key Laboratory for Modification of Chemical Fibers and Polymer Materials, College of Material Science and Engineering, Donghua University, Shanghai, China and

²Engineering Research Center of Advanced Glasses Manufacturing Technology, Ministry of Education, Donghua University, Shanghai, China

Correspondence: Professor H Wang, State Key Laboratory for Modification of Chemical Fibers and Polymer Materials, College of Material Science and Engineering, Donghua University, no. 2999 North Renmin Road, Shanghai, Songjiang 201620, China.

E-mail: wanghz@dhu.edu.cn

or Professor Y Li, Engineering Research Center of Advanced Glasses Manufacturing Technology, Ministry of Education, Donghua University, Shanghai 201620, China.

E-mail: yaogang_li@dhu.edu.cn

Received 14 November 2013; revised 9 May 2014; accepted 1 June 2014

crystalline photoreduced graphene oxide (PRGO) films via a facile illumination treatment. This fabrication method is simple, time-saving and easy to scale up when compared with the previously reported fabrication techniques for scalable-reduced GO films.^{7,13} In this fabrication process, the GO sheets, after derivatization by carboxylic, phenol hydroxyl and epoxide groups, can readily be exfoliated to form a stable colloidal suspension because they are stabilized by their hydrophilicity and electrostatic repulsion,^{14,15} which facilitate the homogeneous arrangement of GO platelets during the preparation of GO films. The subsequent photo-reduction can provide appropriate reduction of the GO films and induce effective interlinking of the individual graphene sheets. Furthermore, we studied the electrochemical performance of PRGO films that serve as electrode material and observed high specific capacitance and mechanical flexibility, thus showcasing their potential application in flexible energy storage devices.

EXPERIMENTAL PROCEDURES

Synthesis of graphite oxide by the Hummers method

All of the reagents used were of analytical grade. Ultrapure water (18.2 M Ω resistance) was used in all experiments. Graphite (3.0 g) was added to concentrated H₂SO₄ (70 ml) under stirring at room temperature, followed by the addition of NaNO₃ (1.5 g) and then the mixture was cooled to 0 °C. Under vigorous agitation, KMnO₄ (9.0 g) was added to the solution slowly. After reaction at 35 °C for 2 h, 150 ml of water was added and the solution was then stirred for 15 min at 98 °C. Successively, the solution was diluted with 1:10 HCl aqueous solution (700 ml), followed by a rapid addition of 400 ml H₂O₂ (3%). The resulting graphite oxide was isolated and washed by vacuum filtration for further use.

Preparation of PRGO films

Three steps were followed to prepare the highly crystalline PRGO films.

Preparation of GO gels: in a typical experiment, 5 ml of as-purified graphite oxide suspensions (10 mg ml⁻¹) were dispersed in water (5 ml) to create a homogeneous dispersion. Exfoliation of graphite oxide to GO was achieved by ultrasonication of the dispersion using a Branson Ultrasonic Cleaner (Branson 3510, 350 W, Emerson, St. Louis, MO, USA) for 1 h and an ultrasonic probe (FS-300, 300 W, Sonix Ultrasonic Instrument, Shanghai, China) for 30 min. The brown dispersion obtained was then subjected to 30 min of centrifugation at 3000 r.p.m. to remove any unexfoliated graphite oxide (usually present in a very small amount) using a centrifuge (5702, Eppendorf, Hamburg, Germany). Next, the GO gels were obtained after increasing the GO concentration by using a rotary evaporator at 45 °C under ~0.09 MPa for 1 h.

Fabrication of GO films: the PRGO films were fabricated by blade coating with an automatic thick-film coater (AFA-III, MTI Corporation, Richmond, CA, USA). Aliquots (2 ml) of the GO gels were dispensed onto the edge area of a piece of Cu foil, and a scraper was pulled over the solution at a speed of 15 mm s⁻¹, leaving a uniform wet film that was then dried under ambient conditions. As a control experiment, chemically converted graphene (CCG) films were prepared using a chemical method to reduce the as-prepared GO films, as reported in previous publications.¹²

Reduction of the GO films by illumination: reduction of the films was performed under illumination using a Xe lamp (XQ350-500W, Shanghai Lansheng Electronic Corporation, Shanghai, China) at room temperature for 0.5~12 h. The PRGO films were cut into the required sizes for various tests. The weight of the whole piece of film was determined after the film was dried at 100 °C for 12 h. The weight of the films was pre-estimated using the actual area of the films. The weight was then checked again after testing (after removing the electrolytes by dialysis and drying). If there was any inconsistency, the value obtained by direct weighing of the tested sample was used.

Characterization

X-ray diffraction (XRD) spectroscopy was performed using a Rigaku D/max 2550V X-ray diffractometer (D/max 2550V, Rigaku, Tokyo, Japan) using Cu-K α irradiation ($\lambda = 1.5406 \text{ \AA}$). The operating voltage and current were

maintained at 40 kV and 300 mA, respectively. The morphologies and the structure of the products were characterized using a high-resolution field emission scanning electron microscope (S-4800, Hitachi, Tokyo, Japan) and a transmission electron microscope (2100 F, JEOL, Tokyo, Japan). Atomic force microscopy images were recorded using a Bruker Dimension 5000 Scanning Probe Microscope in tapping mode (Dimension 5000, Bruker, Camarillo, CA, USA). Raman spectroscopy measurements were performed using a Renishaw Via laser micro-Raman system (Renishaw, Gloucestershire, UK) at an excitation wavelength of 532 nm. The silicon peak at 520 cm⁻¹ was used as a reference. Fourier transform infrared (FTIR) spectra were collected using a Thermo Nicolet NEXUS-670 spectrometer (Nicolet NEXUS-670, Thermo Scientific, Waltham, MA, USA). The KBr pellets for FTIR measurements were prepared by pressing the films and KBr powders using a hand press. The films were supported by transparent polyethylene terephthalate films. X-ray photoelectron spectroscopy measurements were performed using a Kratos AXIS-ultra spectrometer (AXIS-ultra DLD, Kratos, Manchester, UK) equipped with a monochromatic Al-K α X-ray radiation source (1486.71 eV). The dielectric properties of the composite films on fluorine-doped tin oxide-coated glass were measured using a semiconductor device analyzer (E4980A, Agilent, Santa Clara, CA, USA). These measurements were collected at a voltage of 0.1 V and a frequency of 1 kHz.

RESULTS AND DISCUSSION

The typical schematic diagram of the fabrication process of PRGO films is shown in Figure 1a. After ultrasonication and centrifugation treatments, the resulting homogeneous GO solution was concentrated to form stable gels for coating, as shown in Supplementary Figures S1B and S1C. Subsequently, the PRGO films were deposited onto substrates via blade coating using an automatic thick-film coater. Next, the reduction of the films was performed under illumination at ambient temperature for different times. Finally, the PRGO films were cut into different sizes for specified measurements or peeled off to yield free-standing PRGO films. Figure 1b shows a typical image of a PRGO films (8 cm \times 15.5 cm), deposited directly onto a Cu foil substrate that was reduced via the illumination treatment performed for 6 h. The PRGO films in contact with the Cu substrate exhibited a homogeneous shiny graphite luster (Figures 1b, c and e), which indicates the photoreduction of GO to form PRGO and the uniform structure of the fabricated films. In comparison, the GO films exhibit the characteristic reddish-brown color, thus further demonstrating the formation of PRGO films (Supplementary Figure S1A).

Figure 2a schematically illustrates the microstructural transformation occurring in the fabrication procedure, which was revealed by the atomic force microscopy, scanning electron microscopy and transmission electron microscopy (TEM) characterizations. The sizes of the GO nanosheets in GO solution are in the range of nanometers to micrometers, with a typical thickness of approximately 1.1 nm (Supplementary Figure S2). Considering that the thickness of individual GO sheets is approximately 1 nm,^{16,17} the GO in this work is one or two layers, indicating the homogeneous dispersion of GO. However, after PRGO films are formed, the boundary of individual GO nanosheets disappears. Meanwhile, the PRGO film-surface studies (Supplementary Figure S3) clearly indicate that there are some quasi-one-dimensional creases, which were formed by the overlap of GO sheets due to the folding of the GO edges with neighboring sheets during film fabrication. This result is also supported by the cross-sectional scanning electron microscopy image of the wavy PRGO films (Supplementary Figure S4), which were immersed into liquid nitrogen and blown by the released gas. This phenomenon revealed that the edge of one PRGO sheet is entirely in contact with the neighboring sheets and that the sheets are effectively interlinked.

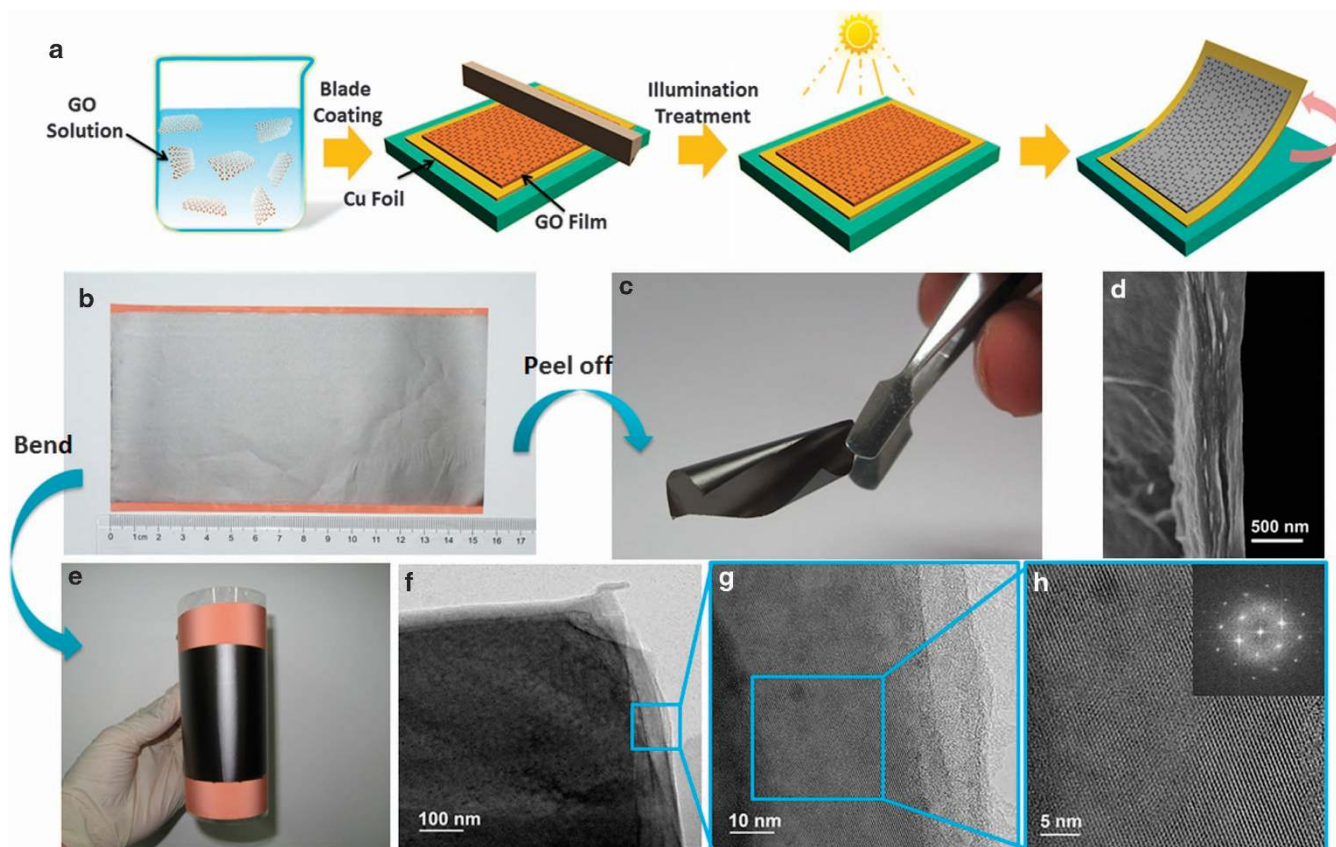


Figure 1 (a) Schematic drawings illustrating the procedures for the fabrication photo-reduced graphene oxide (PRGO) films on Cu foil substrates. (b) A piece of multilayer paper-like PRGO film on a Cu substrate; this film exhibits a shiny graphite luster. (c) A free-standing and flexible PRGO film peeled off from the substrate. (d) Scanning electron microscopy (SEM) image of a cross-section of the paper-like PRGO film. (e) The bent PRGO film on a Cu substrate. (f) Low-magnification transmission electron microscopy (TEM) image of the multilayer PRGO film. (g) Enlarged high-resolution TEM (HRTEM) image of the region marked with a blue rectangle in f. (h) Higher magnification HRTEM image of the PRGO sheet edge. PRGO sheets with clear lattice fringes can be clearly distinguished. The fast Fourier transform (FFT) pattern shown in the inset further demonstrates the highly crystalline nature of PRGO films.

To explore the specific microstructure of the PRGO films, the cross-sectional scanning electron microscopy images of the PRGO films were observed, as shown in Figures 1d and 2b. The morphology exhibits few microcracks, and interspaces between the layers of the PRGO and the GO films (without illustration reduction) are observed in the cross-section images (Supplementary Figures S5A, B, D, E), which is different from the incompact structure of CCG films (Supplementary Figures S5C, F, using the reported method^{12,18}). The well-packed nature of the PRGO sheets was further confirmed by TEM. Supplementary Figures S6A and S6B show TEM images of the GO films, indicating micrometer-scale wrinkles with a loose GO nanosheet structure. In the high-magnification TEM images of the GO films (Supplementary Figures S6C and D), lattice fringes were not obvious because of the random arrangement characteristic of GO sheets. In contrast, Figures 1f and g indicate that the TEM images of PRGO films appear as continuous and tightly stacked edges. In particular, the high-resolution TEM image shown in Figure 1h reveals clear lattice fringes, providing further definitive evidence for the highly crystalline nature of the PRGO films. The inset in Figure 1h clearly shows the diffraction pattern resulting from performing fast Fourier transformation on the image of lattice fringes. This hexagonal pattern shows the typical six-fold symmetry expected for graphene,^{19,20} which also indicates the high in-plane crystallinity of the PRGO sheets. As shown in Supplementary Figure S7, the GO films were immediately dissolved into the solution during 30 s of

ultrasonication. In contrast, the PRGO films remained almost unchanged after the same duration of ultrasonication, which further demonstrated the effective reduction of PRGO sheets.

XRD analyses also provide structural information for both types of samples (Figure 2c), particularly focusing on the crystallinity and interlayer distance. The XRD pattern of the exfoliated GO is characterized by a peak at $2\theta = 11.7^\circ$ with a larger d-spacing of 7.8 Å (compared with the typical value of 3.34 Å in pristine graphite) due to the insertion of hydroxyl and epoxy groups between the carbon sheets and the carboxyl groups along the terminal and lateral sides of the sheets as a result of the oxidation process of graphite. Following the photoreduction process, the XRD pattern of the PRGO films exhibits a sharp peak centered at $2\theta = 26.4^\circ$ and a broad low-intensity peak at $2\theta = 23.8^\circ$, which is most likely due to both the crystalline domain sizes of the graphitic planes and the nature of the expanded graphene sheets, which is consistent with previous TEM results. This peak corresponds to $2\theta = 10.7^\circ$, with an interlayer spacing of 0.82 nm, which is due to the presence of the remaining oxygen-containing groups. In combination with the electron microscopy characterization, the good arrangement of the layer-by-layer structure and the intensive connection between the neighboring sheets, which is induced by photoreduction, is the primary factor that enables the continuous and large-scale manufacturing of PRGO films.

To further identify the composition and crystal structure, we also characterized the PRGO films by means of Raman spectroscopy,

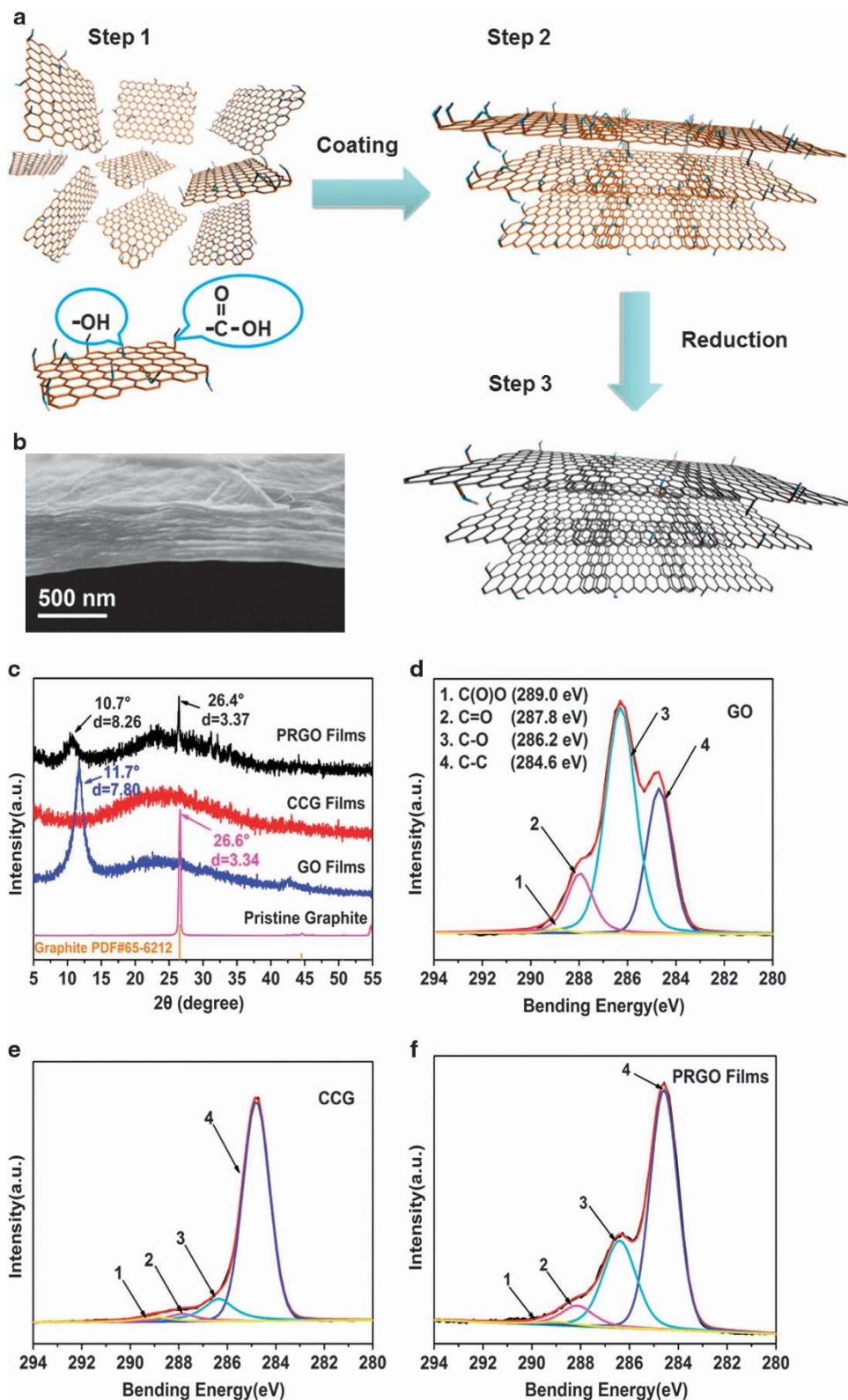


Figure 2 (a) Schematic illustrating the microstructural changes of the photoreduced graphene oxide (PRGO) films for each fabrication procedure. (b) Cross-sectional scanning electron microscopy (SEM) image of a PRGO film. (c) The X-ray diffraction (XRD) patterns of PRGO films, chemically converted graphene (CCG) films, graphene oxide (GO) films and pristine graphite. The interplanar spacings, diffraction peaks and angles are indicated in the figure. Peaks at 10.7° and 26.4° indicate the existence of oxygen-containing groups and highly crystalline regions. (d–f) X-ray photoelectron spectroscopy (XPS) spectra of pure GO films, CCG films and PRGO films, respectively.

X-ray photoelectron spectroscopy and FTIR spectroscopy. The FTIR spectrum (Supplementary Figure S8A) reveals that the intensity of the characteristic peaks corresponding to oxygen-containing chemical groups decreases dramatically after the photoreduction. The decrease is particularly associated with the vibration and deformation peaks of O–H groups at 3421 cm^{-1} and 1400 cm^{-1} , the C=O stretching vibration peak at 1729 cm^{-1} , and the C–O (alkoxy)

stretching vibration peak at 1078 cm^{-1} .¹¹ The X-ray photoelectron spectroscopy technique spectra (Figures 2d–f) were used to investigate the chemical composition and valence states of these films. The broad C1 s peak of the pure GO, CCG and PRGO films can be fitted into four peaks with binding energies at 284.6, 286.2, 287.8 and 289.0 eV, corresponding to the C–C, C–O, C=O and C(O)O groups, respectively.²¹ The peak intensity of the C=O and C–O of the

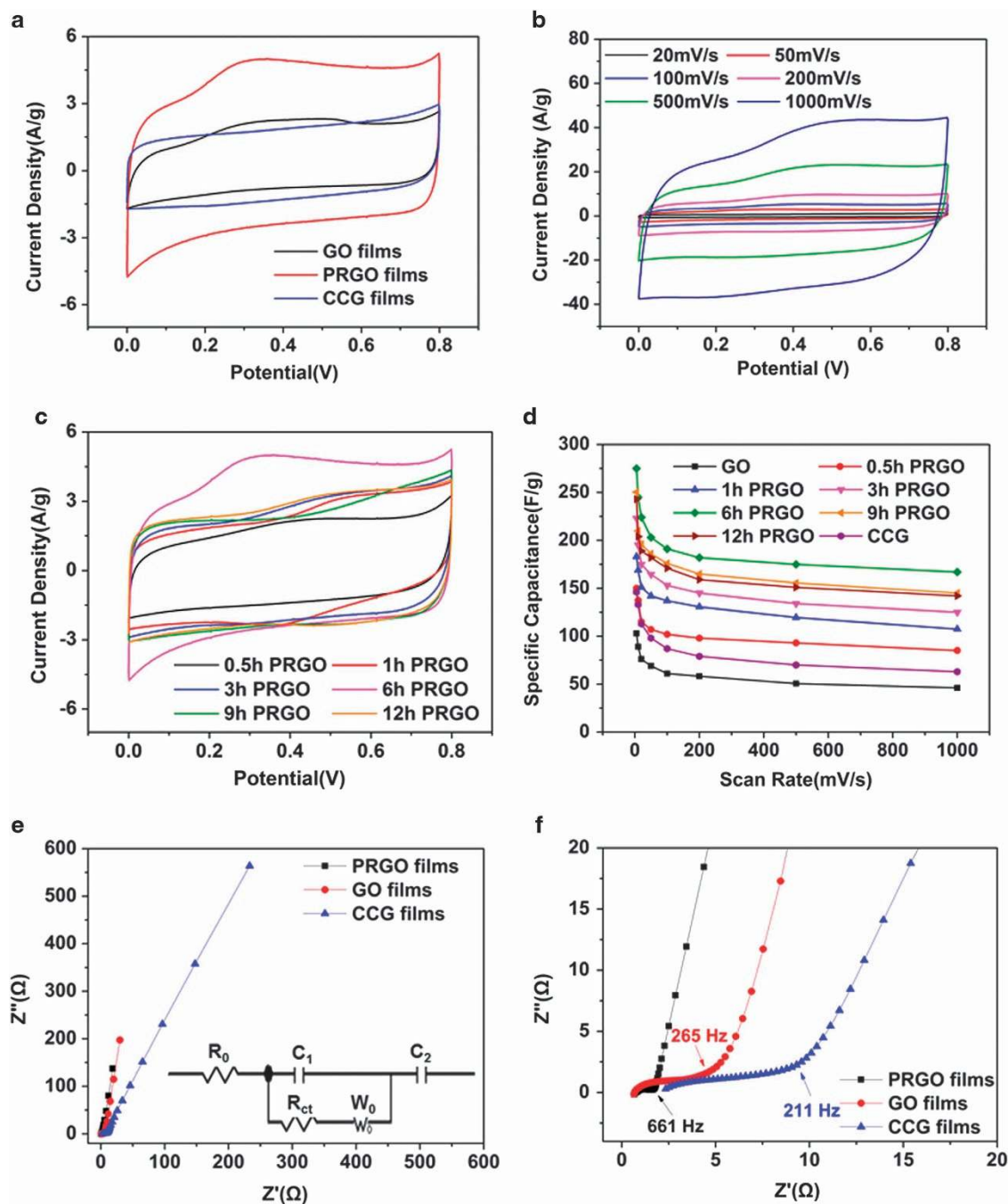


Figure 3 (a) Representative cyclic voltammogram (CV) curves of graphene oxide (GO) films, photoreduced graphene oxide (PRGO) films and chemically converted graphene (CCG) films at a scan rate of 50 mV s^{-1} , (b) CV curves of PRGO films at different scan rates. Even if the scan rate is increased to 1000 mV s^{-1} , the CV curve basically maintains the Faradaic peak-incorporated rectangle-like shape, indicating the high rate capability of PRGO films. (c) CV curves of PRGO films for different illumination times. (d) Calculated specific capacitances from the CV curves at different scan rates of different samples. (e) Nyquist plots of PRGO films, GO films and CCG films; the inset shows the electrical equivalent circuit used for fitting the impedance spectra. (f) The magnified high-frequency regions of the Nyquist curves.

CCG and PRGO films is significantly decreased after photoreduction, which further confirms the successful completion of the reduction process. As seen in Figure 2f, the residual oxygen-containing chemical groups remaining in the PRGO films are mainly due to the incomplete deoxygenation. The change of the electronic structure in the PRGO sheets was further explored by Raman spectroscopy (Supplementary Figure S8B). Analogously, after reduction via light, the intensity ratio of the D band (*ca.* 1340 cm^{-1}) to G band (*ca.* 1590 cm^{-1}), the D/G ratio, increased from 0.96 for the pure GO films to 1.12 for the PRGO films, which is still smaller than the value of 1.35 for the CCG films. The spectroscopic observations thus support the notion that most of the oxygenated groups in the graphitic planes are removed and the sp^2 planes are largely restored; however, a significant number of functional groups at the specific area of the nanosheets are most likely retained. Under illumination, the photothermoelectric effect²² should have a key role in this photoreduction process. The photocurrent induced by the photothermoelectric effect is determined by the photo-induced temperature difference ΔT between the upper surfaces of GO films and the substrate (Supplementary Figure S9). With the photocurrent between the two surfaces of the film, the deoxygenation occurs within almost the entire GO film.

One of the most promising applications of graphene films is their use as electrode material for supercapacitors due to their large specific surface area, high conductivity and excellent electrochemical stability.^{2,23,24} Recently, graphene-based macroscopic films have received increasing attention for use in electrochemical energy storage applications.^{25–29} Despite these examples of significant progress, most of the studies of graphene-based films for use in supercapacitors to date involved the fabrication of free-standing graphene films or the preparation of electrodes with the binder first and then the transfer of the electrode film onto current collector (conductive substrate, for example, platinum, gold or copper foil); such processes introduce high contact resistance between the electrode and the current collector, which result in significant loss of storage and transmission capacity. Our PRGO films are directly coated onto conductive substrate, which advantageously minimizes the contact resistance, thus enabling the double-layer charges to be conveniently transferred to the current collector to cause the partial reduction of GO films and to further enhance the capacitance performance.³⁰

A symmetrical two-electrode system was used to characterize the electrochemical characteristics of the as-fabricated PRGO films in comparison with those of the GO films and the CCG films. Figure 3a shows the cyclic voltammograms (CVs) of the PRGO films, the GO films and the CCG films in 1 mol l^{-1} Na_2SO_4 aqueous solutions for applied potentials between 0 V and 0.8 V at a scan rate of 50 mV s^{-1} . The CV curves of CCG films exhibit a typical rectangular shape, implying pure electric double-layer capacitive behavior. In contrast, the CV curves of both GO and PRGO films exhibit a box-like shape superimposed with a well-broadened peak at 0.2–0.6 V, indicating the coexistence of electric double-layer capacitance and pseudocapacitance. The deviations of the CV curves at specific potential regions are related to the rapid Faradaic reactions, which may be correlated to the presence of additional oxygen-containing functional groups, especially epoxy and alkoxy, at the surface of the carbon.^{27,30} PRGO films exhibit the largest current density in the CV curves, implying a larger capacitance than those of the GO and CCG films. Figure 3b shows the CV curves of the PRGO films at different scan rates. Even when the scan rate increases to 1000 mV s^{-1} , the CV curve basically maintains the Faradaic peak-incorporated rectangular shape, similar to that observed at 20 mV s^{-1} , which is indicative of the rapid charge-

propagation capability of both the electric double-layer capacitance and the pseudocapacitance in the PRGO electrode. The specific capacitances at different scan rates are calculated based on the CV measurements. The highest capacitance of 275 F g^{-1} were achieved for the PRGO films at scan rate of 10 mV s^{-1} , which are exceptionally higher than the values of the GO films (103 F g^{-1}), the CCG films (146 F g^{-1}) and those reported previously for graphene.^{23,28,31} Furthermore, on increasing the scan rate up to 1000 mV s^{-1} , the specific capacitance remain stable at 167 F g^{-1} , highlighting the excellent rate capability of PRGO films. We compared the capacitance performances of the PRGO films with those of recent research works focused on graphene-based films for supercapacitors by examining the data presented in Supplementary Tables S2 and S3. The PRGO films outperform these typical pure CCG-based carbon materials in terms of high capacitance. Moreover, the performance of PRGO films is even comparable with those of doped or functionalized graphene-based electrodes. Partial oxygen-containing groups on PRGO films were retained during the photoreduction process, which was confirmed by XRD, FTIR and XPS analysis, as presented above. The partially retained oxygen-containing groups are advantageous, as they can provide a large additional pseudocapacitance as well as improved wettability, providing PRGO films with a higher capacitance than that of the CCG films. In contrast to the current density of the PRGO films, the current density in the CV curve of the GO films is not as high, although the content of the oxygen-containing groups in the GO films is notably higher than that in the PRGO films. The reason that the PRGO films possess a much higher capacitance than the GO electrode is most likely due to the intensively stacked highly crystalline structure of the PRGO films and the reduced graphene regions, which lead to a dramatic increase in the electrical conductivity along the vertical direction of the electrode. In addition, we believe that the polarization occurring on the surface of the electrode material could be another important factor for enhanced capacitance. In PRGO films, the neighboring conductive PRGO platelets and partially reduced PRGO sheets with the remaining oxygen-containing groups in between the sheets could result in interfacial polarization, which leads to internal barrier layer capacitors.³² In general, interfacial polarization can lead to the enhancement of the dielectric constant. Thus, we tested the dielectric constant of different films to confirm the interfacial polarization influence on the capacitance. The PRGO film exhibited a higher dielectric constant than those of the GO and CCG films (Supplementary Table S1). Therefore, we conclude that the increase of the dielectric constant induced by interfacial polarization is another key factor for the enhancement the electrochemical performance of PRGO films.

To evaluate the influence of photoreduction on the capacitance of the PRGO films, we performed a detailed study of the impact of the illumination time (0.5–12 h) within a large range of the scan rates on the capacitance. As shown in Figure 3c, we obtained CV curves of the PRGO films formed using different illumination times ranging from 0.5 to 12 h at a scan rate of 50 mV s^{-1} . The current response increases with a rise in illumination time at time range from 0.5 to 6 h, indicating an enhancement of the total capacitance. However, with the continued lengthening of the illumination time, the current density exhibits a slight decrease. The decrease of the specific capacitances with increasing illumination time may due to the additional illumination, leading to the decrease in the content of oxygen-containing functional groups. The decrease could result in the decrease of pseudocapacitive reactions, as indicated by the weakened peak of the CV curves. The specific capacitances of PRGO films formed by reduction over different times, GO films and CCG films

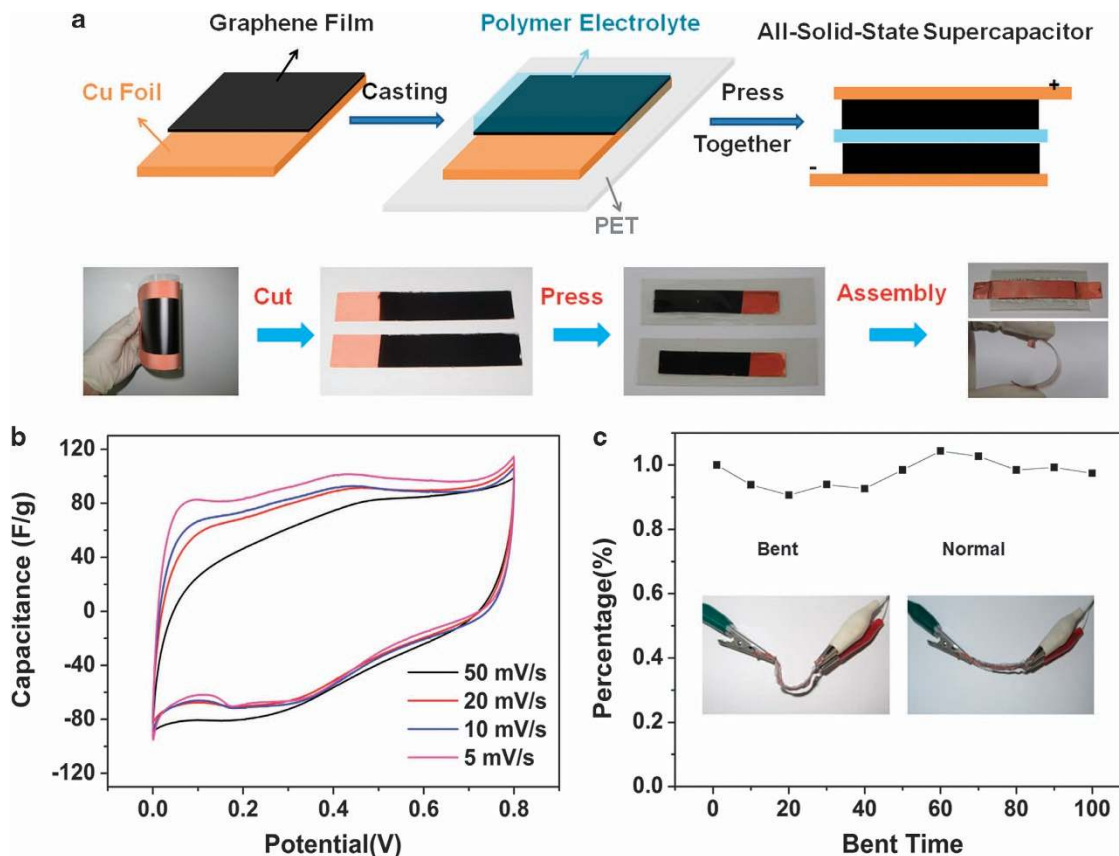


Figure 4 (a) Schematic diagram and photographs of the fabrication process of flexible all-solid-state supercapacitors based on photoreduced graphene oxide (PRGO) films. (b) Cyclic voltammogram (CV) curves of all-solid-state supercapacitors at different scan rates. (c) Cycling stability of the all-solid-state supercapacitors under repeated bending/extending tests.

are plotted in Figure 3d. The specific capacitance of the PRGO films with illumination of 6 h is higher than those of all other samples, which indicate that the 6-h reduction is the optimal experimental condition for fabricating supercapacitor electrodes.

Further electrochemical investigation was performed to determine the frequency response as well as the equivalent series resistance of the symmetrical two-electrode measurement system based on the fabricated materials. The electrochemical impedance spectroscopy plots of the PRGO, GO and CCG films are shown in Figures 3e and f. In the low-frequency portion of the spectrum of the PRGO films and the GO films, both impedance spectra tend toward a vertical line, where the imaginary part of impedance rapidly increases, which is characteristic of capacitive behavior due to the ion diffusion in the electrode structure. In comparison, the CCG films exhibit an expanded Warburg region, reflecting slow ion transport. The knee frequency is used to evaluate the frequency dependence of a capacitor and is considered to be the critical frequency at which supercapacitors begin to exhibit capacitive behavior. As shown in Figure 3f, the knee frequency of the PRGO films is over 660 Hz, indicating that most of its stored energy is accessible at frequencies below 660 Hz, whereas the knee frequencies of the GO and CCG films are much lower, at 265 Hz and 211 Hz, respectively. The knee frequencies of the PRGO films are much higher than some of the reported values for the graphene and carbon nanotube electrodes,^{33,34} which could be the result of rapid electrolyte ions access and diffusion through the conductive paths and the GO sheets. In the high-frequency region, the first intersections of the curves with the real axis indicate the ohmic resistance R_0 or the

equivalent series resistance, which represents the sum of the resistance of the electrolyte, the intrinsic resistance of the electrode materials, and the contact resistance between the interfaces of electrode material, electrolyte, and current collector.³¹ The measured impedance spectra were analyzed based on an equivalent circuit, which is shown in the inset of Figure 3e. The calculated ohmic resistance R_0 of the PRGO films and the GO films were estimated to be quite low values of 0.89Ω and 0.92Ω , respectively, in contrast to 2.47Ω for the CCG films, indicating the well-connected nature of the interfaces of the electrode films, electrolyte ions, and current, due to the intensive contact between the electrode films and conductive substrate and the improved wettability provided by the oxygen-containing groups.

To demonstrate the performance of the fabricated PRGO electrodes for use in flexible energy storage, we finally assembled all-solid-state flexible supercapacitors using PRGO films as an active electrode material. Figure 4a shows the processing steps used to fabricate PRGO film-based solid-state flexible supercapacitors. To assemble the solid-state supercapacitor device, H_2SO_4 /polyvinyl alcohol gel was used as the electrolyte, which would additionally protect the PRGO micro-patterned electrodes from wear and breakage due to its excellent mechanical integrity.³³ The fabricated device was highly flexible and robust. The capacitive performance of the flexible solid-state supercapacitors was evaluated by CV (Figure 4b). In general, the shape of the CV loop also exhibits the Faradaic peak-incorporated rectangular shape, similar to that observed in the previous analysis, which indicates that the capacitance combined both the electric double-layer capacitance and the pseudocapacitance in the PRGO

electrode. The specific capacitance of the graphene hydrogel film electrode estimated from the CV curves was 130 F g^{-1} , which is substantially higher than those of most of the previously reported solid-state devices made of carbon nanotubes ($50\text{--}115 \text{ F g}^{-1}$),^{35,36} and graphene films ($62\text{--}120 \text{ F g}^{-1}$).^{37–39} A long mechanical stability is an important concern for practical applications of flexible all-solid-state supercapacitors. To investigate the mechanical stability of as-prepared PRGO all-solid-state supercapacitors, CV cycling tests were performed at a scan rate of 50 mV s^{-1} for 100 bending cycles. As shown in Figure 4c, the capacity decay is only 2% of the initial discharge capacity, indicating the excellent mechanical stability of the PRGO-based all-solid-state supercapacitors.

CONCLUSIONS

In conclusion, we have fabricated large-scale and flexible films of highly crystalline and intensively stacked structures directly onto conductive substrates via a facile coating and subsequent illumination method. Through the coating process and photoreduction, GO platelets were reconstructed to form layer-by-layer-stacked PRGO films. This method has the advantages of being a fast, simple process that is high throughput, and low cost for the preparation of large-area, high-quality PRGO films directly onto conductive supports or substrates. Compared with previously reported scalable-reduced GO films, PRGO films exhibit greatly improved performance as flexible electrode materials for supercapacitors. The PRGO films exhibited an 88% increase in specific capacitance compared with that of CCG films, mainly due to the minimized contact resistance and the additional pseudocapacitance. In addition, the interfacial polarization between the neighboring graphene platelets and the nonconductive GO sheets plays a crucial role in the enhancement of the capacitance, although the exact chemistry behind this phenomenon requires further study. Because of the scalable synthesis and the demonstrated promising properties, these PRGO films are promising for use in applications in flexible electronics devices.

CONFLICT OF INTEREST

The authors declare no conflict of interest.

ACKNOWLEDGEMENTS

We gratefully acknowledge the financial support given by the Natural Science Foundation of China (No. 51172042), the Specialized Research Fund for the Doctoral Program of Higher Education (20110075130001), the Science and Technology Commission of the Shanghai Municipality (12nm0503900, 13JC1400200), the Program for Professor of Special Appointment (Eastern Scholar) at the Shanghai Institutions of Higher Learning, the Innovative Research Team in University (IRT1221), the Program of Introducing Talents of Discipline to Universities (No.111-2-04) and Donghua University (CUSF-DH-D-2013009). We thank Professor Richard Kaner of UCLA for valuable suggestions and helpful discussions.

- Rogers, J. A., Someya, T. & Huang, Y. Materials and mechanics for stretchable electronics. *Science* **327**, 1603–1607 (2010).
- El-Kady, M. F. & Kaner, R. B. Scalable fabrication of high-power graphene micro-supercapacitors for flexible and on-chip energy storage. *Nat. Commun.* **4**, 1475 (2013).
- Allen, M. J., Tung, V. C. & Kaner, R. B. Honeycomb carbon: a review of graphene. *Chem. Rev.* **110**, 132–145 (2009).
- Dai, L. M. Functionalization of graphene for efficient energy conversion and storage. *Acc. Chem. Res.* **46**, 31–42 (2012).
- Zhang, Y., Zhang, L. & Zhou, C. Review of chemical vapor deposition of graphene and related applications. *Acc. Chem. Res.* **46**, 2329–2339 (2013).

- Pham, V. H., Cuong, T. V., Hur, S. H., Shin, E. W. & Kim, J. S. Fast and simple fabrication of a large transparent chemically-converted graphene film by spray-coating. *Carbon*. **NY** **48**, 1945–1951 (2010).
- Wang, J., Liang, M. H., Fang, Y., Qiu, T. F., Zhang, J. & Zhi, L. J. Rod-coating: towards large-area fabrication of uniform reduced graphene oxide films for flexible touch screens. *Adv. Mater.* **24**, 2874–2878 (2012).
- Becerril, H. A., Mao, J., Liu, Z. F., Stoltenberg, R. M., Bao, Z. N. & Chen, Y. S. Evaluation of solution-processed reduced graphene oxide films as transparent conductors. *ACS Nano* **2**, 463–470 (2008).
- Güneş, F., Shin, H. J., Biswas, C. D., Han, G. H., Kim, E. S., Chae, S. J., Choi, J. Y. & Lee, Y. H. Layer-by-layer doping of few-layer graphene film. *ACS Nano* **4**, 4595–4600 (2010).
- Li, X., Zhang, G. Y., Bai, X. D., Sun, X. M., Wang, X. R., Wang, E. G. & Dai, H. J. Highly conducting graphene sheets and Langmuir-Blodgett films. *Nat. Nanotechnol.* **3**, 538–542 (2008).
- Gan, S., Zhong, L. J., Wu, T. S., Han, D. X., Zhang, J. D., Ulstrup, J., Chi, Q. J. & Niu, L. Spontaneous and fast growth of large-area graphene nanofilms facilitated by oil/water interfaces. *Adv. Mater.* **24**, 3958–3964 (2012).
- Li, D., Muller, M. B., Gilje, S., Kaner, R. B. & Wallace, G. G. Processable aqueous dispersions of graphene nanosheets. *Nat. Nanotechnol.* **3**, 101–105 (2008).
- Cao, X., Qi, D. P., Yin, S. Y., Bu, J., Li, F. J., Goh, C. F., Zhang, S. & Chen, X. D. Ambient fabrication of large-area graphene films via a synchronous reduction and assembly strategy. *Adv. Mater.* **25**, 2957–2962 (2013).
- Luo, J., Kim, J. & Huang, J. Material processing of chemically modified graphene: some challenges and solutions. *Acc. Chem. Res.* **46**, 2225–2234 (2013).
- Raidongia, K. & Huang, J. Nanofluidic ion transport through reconstructed layered materials. *J. Am. Chem. Soc.* **134**, 16528–16531 (2012).
- Jung, I., Dikin, D. A., Piner, R. D. & Ruoff, R. S. Tunable electrical conductivity of individual graphene oxide sheets reduced at 'low' temperatures. *Nano Lett.* **8**, 4283–4287 (2008).
- Eda, G. & Chhowalla, M. Chemically derived graphene oxide: towards large-area thin-film electronics and optoelectronics. *Adv. Mater.* **22**, 2392–2415 (2010).
- Cao, H., Li, C. & Shi, G. Functional composite materials based on chemically converted graphene. *Adv. Mater.* **23**, 1089–1115 (2011).
- Hernandez, Y., Nicolosi, V., Lotya, M., Blighe, F. M., Sun, Z. Y., De, S., McGovern, I. T., Holland, B., Byrne, M., Gun'ko, Y. K., Boland, J. J., Niraj, P., Duesberg, G., Krishnamurthy, S., Goodhue, R., Hutchison, J., Scardaci, V., Ferrari, A. C. & Coleman, J. N. High-yield production of graphene by liquid-phase exfoliation of graphite. *Nat. Nanotechnol.* **3**, 563–568 (2008).
- Gu, W., Zhang, W., Li, X. M., Zhu, H. W., Wei, J. Q., Li, Z., Shu, Q. K., Wang, C., Wang, U. L., Shen, W. C., Kang, F. Y. & Wu, D. H. Graphene sheets from worm-like exfoliated graphite. *J. Mater. Chem.* **19**, 3367–3369 (2009).
- Dreyer, D. R., Park, S., Bielawski, C. W. & Ruoff, R. S. The chemistry of graphene oxide. *Chem. Soc. Rev.* **39**, 228–240 (2010).
- Gabor, N. M., Song, J. C. W., Ma, Q., Nair, N. L., Taychatanapat, T., Watanabe, K., Taniguchi, T., Levitov, L. S. & Herrero, P. J. Hot carrier-assisted intrinsic photoresponse in graphene. *Science* **334**, 648–652 (2011).
- Stoller, M. D., Park, S., Zhu, Y., An, J. & Ruoff, R. S. Graphene-based ultracapacitors. *Nano Lett.* **8**, 3498–3502 (2008).
- Yang, X., Zhu, J., Qiu, L. & Li, D. Bioinspired effective prevention of restacking in multilayered graphene films: towards the next generation of high-performance supercapacitors. *Adv. Mater.* **23**, 2833–2838 (2011).
- Xu, C., Xu, B. H., Gu, Y., Xiong, Z. G., Sun, J. & Zhao, X. S. Graphene-based electrodes for electrochemical energy storage. *Energy Environ. Sci.* **6**, 1388–1414 (2013).
- Wen, Z., Wang, X. C., Mao, S., Bo, Z., Kim, H. J., Cui, S. M., Lu, G. H., Feng, X. L. & Chen, J. H. Crumpled nitrogen-doped graphene nanosheets with ultrahigh pore volume for high-performance supercapacitor. *Adv. Mater.* **24**, 5610–5616 (2012).
- Fang, Y., Luo, B., Jia, Y. Y., Li, X. L., Wang, B., Song, Q., Kang, F. Y. & Zhi, L. J. Renewing functionalized graphene as electrodes for high-performance supercapacitors. *Adv. Mater.* **24**, 6348–6355 (2012).
- Li, Y., Li, Z. & Shen, P. K. Simultaneous formation of ultrahigh surface area and three-dimensional hierarchical porous graphene-like networks for fast and highly stable supercapacitors. *Adv. Mater.* **25**, 2474–2480 (2013).
- Chen, J., Sheng, K., Luo, P., Li, C. & Shi, G. Graphene hydrogels deposited in nickel foams for high-rate electrochemical capacitors. *Adv. Mater.* **24**, 4569–4573 (2012).
- Xu, B., Yue, S. F., Sui, Z. Y., Zhang, X. T., Hou, S. S., Cao, G. P. & Yang, Y. S. What is the choice for supercapacitors: graphene or graphene oxide? *Energy Environ. Sci.* **4**, 2826–2830 (2011).
- Luo, J., Jang, H. D. & Huang, J. Effect of sheet morphology on the scalability of graphene-based ultracapacitors. *ACS Nano* **7**, 1464–1471 (2013).
- Kim, J. Y., Lee, W. H., Suk, J. W., Potts, J. R., Chou, H., Kholmanov, I. N., Piner, R. D., Lee, J., Akinwande, D. & Ruoff, R. S. Chlorination of reduced graphene oxide enhances the dielectric constant of reduced graphene oxide/polymer composites. *Adv. Mater.* **25**, 2308–2313 (2013).
- Niu, Z., Zhang, L., Liu, L. L., Zhu, B. W., Dong, H. B. & Chen, X. D. All-solid-state flexible ultrathin micro-supercapacitors based on graphene. *Adv. Mater.* **25**, 4035–4042 (2013).
- Zhang, C., Peng, Z. W., Lin, J., Zhu, Y., Ruan, G. D., Hwang, C. C., Lu, W., Hauge, R. H. & Tour, J. M. Splitting of a vertical multiwalled carbon nanotube carpet to a graphene nanoribbon carpet and its use in supercapacitors. *ACS Nano* **7**, 5151–5159 (2013).

- 35 Kaempgen, M., Chan, C. K., Ma, J., Cui, Y. & Gruner, G. Printable thin film supercapacitors using single-walled carbon nanotubes. *Nano Lett.* **9**, 1872–1876 (2009).
- 36 Hu, S., Rajamani, R. & Yu, X. Flexible solid-state paper based carbon nanotube supercapacitor. *Appl. Phys. Lett.* **100**, 104103–104104 (2012).
- 37 Choi, B. G., Hong, J., Hong, W. H., Hammond, P. T. & Park, H. Facilitated ion transport in all-solid-state flexible supercapacitors. *ACS Nano* **5**, 7205–7213 (2011).
- 38 Choi, B. G., Chang, S. J., Kang, H. W., Park, C. P., Kim, H. J., Hong, W. H., Lee, S. G. & Huh, Y. S. High performance of a solid-state flexible asymmetric supercapacitor based on graphene films. *Nanoscale* **4**, 4983–4988 (2012).
- 39 Weng, Z., Su, Y., Wang, D. W., Li, F., Du, J. H. & Cheng, H. M. Graphene–cellulose paper flexible supercapacitors. *Adv. Energy Mater.* **1**, 917–922 (2011).



This work is licensed under a Creative Commons Attribution-NonCommercial-NoDerivs 3.0 Unported License. The images or other third party material in this article are included in the article's Creative Commons license, unless indicated otherwise in the credit line; if the material is not included under the Creative Commons license, users will need to obtain permission from the license holder to reproduce the material. To view a copy of this license, visit <http://creativecommons.org/licenses/by-nc-nd/3.0/>

Supplementary Information accompanies the paper on the NPG Asia Materials website (<http://www.nature.com/am>)